Journal of Materials Chemistry C

ARTICLE

Plasmonic Nanopillar Arrays Encoded with Multiplex Molecular Information for Anti-counterfeiting Applications

Y. Liu,[a] Y. H. Lee,[a] Q. Zhang,[a] Y. Cui[a] and X. Y. Ling[a]*

Received 00th January 20xx,
Accepted 00th January 20xx

DOI: 10.1039/x0xx00000x

www.rsc.org/

A major challenge in information security and developing anti-counterfeiting platform is to encode multiple identification features which can be decoded with no interference on a single platform. Here, we demonstrate a progressively complex anti-counterfeiting platform using a multiplex fabrication strategy. This multiplex strategy enables us to realize the spatially selective encapsulation of dye molecules within a Ag nanopillar array, embedding covert molecular information which are revealed in the form of fluorescence, surface-enhanced Raman scattering (SERS), and signal intensities. A total of five identification layers can be used to authenticate genuine products in our nanopillar platform. Moreover, two spectroscopic techniques are required to fully decode the various covert layers encoded within the same nanopillar array, thereby greatly enhances the information security. Hyperspectral imaging technique precisely generates unique SERS fingerprints of molecules encapsulated in each nanopillars, making our anti-counterfeiting platform extremely difficult to be forged when combining with high information density of ~17,000 pillars per inch (ppi). Our encoding platform enables high security, large information density and low-error decoding.

1. Introduction

There is vast amount of digital information generated daily (~2.5×10^{18} bytes) in modern society.[1] Effective protection of these data against unwanted or accidental information thefts is increasingly important in a digital era. Information security entails encoding information such that only authorized parties can read it; decoding involves the use of advanced and complicated spectroscopic techniques which are not readily accessible by the general public. On the other hand, fast-growing product forgery causes enormous financial damage and threatens public health, driving immediate urgency in developing complex anti-counterfeiting platforms. Nanoparticles and nanostructures are promising materials for information security and anti-counterfeiting: their small dimensions and unique optical properties enable encoding of high-density information which can be read out by using advanced analytical instruments as identification. For example, structural colors,[2-7] fluorescence/photoluminescence,[8-10] and surface-enhanced Raman scattering (SERS)[11-13] are some commonly used techniques for security labels. However, the optical signal outputs of the stored information in these nanostructures depend strongly on their physical features (morphology and structural orientations). Minor changes in physical features during fabrication can lead to false signals. Furthermore, these physical features are easily discernible under optical or electron microscopy, implying that these platforms are unable to securely hide the data stored.

To further secure information and deter forgery, additional optical features are always embedded within the physical features. Multiplexing is an attractive approach to incorporate multiple features within a single platform which can subsequently be selectively and individually read out. These optical features are independent of nanostructure morphology, and can only be fully decoded using any of the aforementioned spectroscopic techniques chosen by the authorized parties.[14-19] However, these systems primarily use one read-out technique per platform. Security level can be further increased by using a platform with multiple layers of identification features to distinguish between authentic and fake products. To achieve a multiple-layer encoding platform using a multiplexing strategy, the major challenge is to prevent signal interferences among multiple features and obtain low-error readouts using various spectroscopic techniques in the multiplex system.

Here, we demonstrate a multiple-layer anti-counterfeiting platform with enhanced information security using a multiplex fabrication strategy. The aim is to develop an information encoding platform with large information density, high security and low-error decoding. A progressively complex anti-counterfeiting platform is achieved by utilizing arrays of

[a] Division of Chemistry and Biological Chemistry, School of Physical and Mathematical Sciences, Nanyang Technological University, 637371, Singapore. E-mail: xyling@ntu.edu.sg

†Electronic Supplementary Information (ESI) available: Comparison on morphologies of photoresist nanopillar and dye-encapsulated nanopillars, homogeneity of SERS and fluorescence signals on dye-encapsulated nanopillars, SERS spectra comparison between commercial photoresist IPL-780 and our photoresist, fluorescence intensity grayscales and SERS intensity profile of the nanopillar array, influence of Ag thickness in the multiplex array, fluorescence and SERS taken from the multiplex nanopillar array, comparison on SERS taken from the multiplex system and single-dye system, zoom-in SERS taken from R6G- (orange) and EY-encapsulated nanopillars (blue) in 'yin-yang' pattern and assignment of major vibrational peaks in SERS spectra of R6G- and EY-encapsulated nanopillars. See DOI: 10.1039/x0xx00000x

nanopillars fabricated using two-photon photolithography, where multiple identification layers of molecular information are read out in the form of fluorescence, SERS, and their signal intensities. In addition, we create covert nanoscale patterns by devising a protocol to selectively encapsulate multiple dye molecules (multiplex) over different areas of the same substrate. These images can only be fully decoded using both fluorescence and SERS hyperspectral imaging. Decoding accuracy is enhanced due to the independence of optical readouts from the physical features. Furthermore, the combination of the high information density that is ~17,000 pillars per inch with hyperspectral imaging technology indicates that ~17,000 complete spectral information can be fully decoded within every inch. This further enhances accuracy of data outputs and the information security.

2. Experimental Section

2.1 Materials

Rhodamine 6G, eosin Y and dimethyl sulfoxide were purchased from Sigma Aldrich. Milli-Q water (> 18.0 MΩ•cm) was purified with a Sartorius Arium 611 UV ultrapure water system.

2.2 Synthesis of photoresist

Methyl 2-(methyl(phenyl)amino)acetate

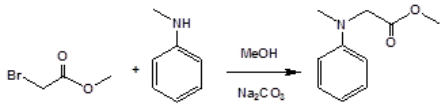

In a 100 mL flask, 3.05 mL of methyl bromoacetate, 3.975 g of sodium carbonate and 2.725 mL of N-methylaniline were dissolved in 37.5 mL of methanol. The reaction mixture was stirred under reflux at 75 °C for 3.5 h. Then the solution was filtered off, the solid residue was washed with ethylacetate (EA, 3 × 30 mL). The solution was washed with water (3 × 100 mL) and brine (1 × 100 mL). The organic layer was dried over sodium sulfate, filtered and concentrated. Purification by column chromatography (Hexane: EA=20:1) yielded 2.473 g (66%) of the desired products as light yellow oil.

^{1}H-NMR (200 MHz, $CDCl_3$, δ): 7.51 – 7.10 (m, 2H), 6.85 – 6.74 (m, 3H), 4.14 (s, 2H), 3.77 (s, 3H), 3.13 (s, 3H); ^{13}C-NMR (50 MHz, $CDCl_3$, δ): 171.6, 148.8, 129.2, 117.4, 112.3, 54.3, 51.9, 39.5; GS-MS *m/z*: 179.20, 120.16, 91.11, 77.08.

Methyl 2-((4-formylphenyl)(methyl)amino)acetate

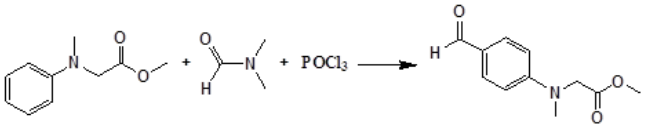

1.15 mL of phosphorous oxychloride (25 mmol) were dropwisely added to 10 mL of dry DMF at 0 °C. After 30 min, 2.24 g of methyl 2-(methyl(phenyl)amino)acetate (25 mmol) were added to the reaction mixture, which was subsequently heated to 75 °C for 4h. Then the solution was cooled and poured into ice water (250 mL) with vigorous stirring overnight. The mixture was extracted with methylene chloride (3 × 50 mL) and the combined organic layers were washed with water (3 × 50 mL) and brine (1 × 50 mL). Then the organic layer was dried over sodium sulfate. The solvent was evaporated and the crude product was purified by column chromatography (Hexane: EA=2:1) to yield 1.8 g (69%) of products as white solid. Mp: 75-78 °C.

^{1}H-NMR (200 MHz, $CDCl_3$): δ (ppm) = 9.68 (s, 1H), 7.66 (d, J = 8.9 Hz, 2H), 6.62 (d, J = 8.9 Hz, 2H), 4.09 (s, 2H), 3.66 (s, 3H), 3.07 (s, 3H). ^{13}C-NMR (50 MHz, $CDCl_3$): δ (ppm) = 190.39, 170.26, 153.34, 131.98, 126.34, 111.37, 53.84, 52.25, 39.65. GS-MS analysis: (m/z) = 207.28, 148.22, 118.20, 77.10.

Sodium 2-((4-formylphenyl)(methyl)amino)acetate

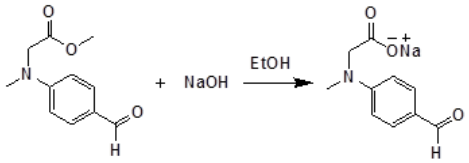

A mixture of methyl 2-((4-formylphenyl)(methyl)amino)acetate (1g, 4.82 mmol) and NaOH powder (0.6g, 15 mmol) in 20 mL of EtOH was stirred overnight at room temperature. The solvent was removed in vacuum and the crude product was used directly for the next step without further purification.

Photoresist monomer

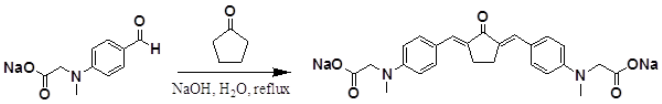

With protection of Al foil, 0.01 g of sodium hydroxide, 0.978 g of the benzaldehyde compound and 0.181 g of freshly distilled cyclopentanone were dissolved in 10 mL of water. The reaction was stirred at 80 °C for 4 h and then cooled to room temperature. 20 mL of EtOH and 1 M HCl were added consequently until no precipitate formed. The red solids were collected by centrifugation and dried in vacuum. The obtained solids were put into 20 mL of water and 0.1 M NaOH was added dropwise until pH 8.5 was reached (monitored with pH meter). The undissolved solids were filtered off and water was removed via freeze-drying to yield desired products 0.966 g (88% of two steps).

2.3 Surface-enhanced Raman scattering (SERS) measurements

SERS spectra and SERS mapping were obtained using Ramantouch microspectrometer (Nanophoton, Osaka, Japan). A 532 nm laser was used as the excitation laser. The laser power used for the measurements is 10 μW. The damage power to the substrate is 20 μW where the organic molecules are burnt. The excitation laser light was focused into a line on a sample through a cylindrical lens and an air objective lens (LU Plan Fluor 100× NA 0.9). The back-scattered Raman signal from the line illuminated site was collected with the same objective lens, and a one-dimensional Raman image (1D space and Raman spectra) was obtained with a two-dimensional image sensor (pixis 400 BR,-70 °C, 1340 × 400 pixels) at once. Two-dimensional (2D)

Raman spectral images were obtained by scanning the line-shaped laser focus in a single direction. The exposure time for each line and slit width of the spectrometer were 1 s and 50 µm for 2D Raman imaging. The line scan mode with the resolution of y direction around 300 nm was used for x-y imaging.

2.4 Fluorescence measurements

A 532 nm laser was used as an excitation laser with the laser power of 10 µW. The excitation laser light was focused into a line on a sample through a cylindrical lens and an air objective lens (LU Plan Fluor 100× NA 0.9). The exposure time for each line of the spectrometer were 1 s. The line scan mode with the resolution of y direction around 300 nm was used for x-y imaging.

2.5 Characterization

Scanning electron microscope (SEM) was performed using a JEOL-JSM-7600F with an accelerating voltage of 5 kV.

3. Results and Discussion

3.1 Nanopillar Fabrication

We fabricate arrays of structurally identical nanopillars for our anti-counterfeiting platform using two-photon photolithography. A benzylidene ketone-based photoresist serves as both photo-initiator and monomer (Scheme 1). Dye molecules such as rhodamine 6G (R6G) and eosin Y (EY) can be easily encapsulated within the nanopillars by mixing the dye solution with the photoresist prior to the laser writing process. Following photo-polymerization, the nanopillars are rendered SERS-active by thermally evaporating 25 nm of Ag layer (Scheme 1). The SERS signals are detected because of the nanoscale asperities serving as hot spots generated by the thermal evaporation process and 532-nm laser generates sufficient near-field enhancements to enhance the Raman signals on these nanoscale asperities.[11, 19] Photolithography enables us to achieve high structural fidelity and precision in the fabrication of the dye encapsulated nanopillar arrays (Fig. 1A, B). The diameters of the Ag coated nanopillars are 520 ± 20 nm (Fig. 1A, B), with average heights of 1.1 ± 0.1 µm (Fig. 1C, D). The plasmon bands of these Ag coated nanopillars with large sizes and dielectric cores are predicted to be in the near- and mid-infrared region.[20-22] Thermal evaporation of Ag generates nanoscale asperities serving as hot spots for SERS detection on the surfaces of nanopillars.[11, 19] In addition, the presence of dye molecules does not affect the fabrication of the nanopillars (Fig. S1, ESI†).

We then investigate the information encoding capability of the nanopillar arrays, making use of 2D hyperspectral imaging spectroscopy to retrieve the embedded fluorescence and SERS information. The fluorescence images of the R6G- and EY-encapsulated nanopillars demonstrate uniform fluorescence intensity when the emission peaks of R6G and EY are selected at 560 nm and 630 nm, respectively (Fig. 1E, F, S2A, B, ESI†). In

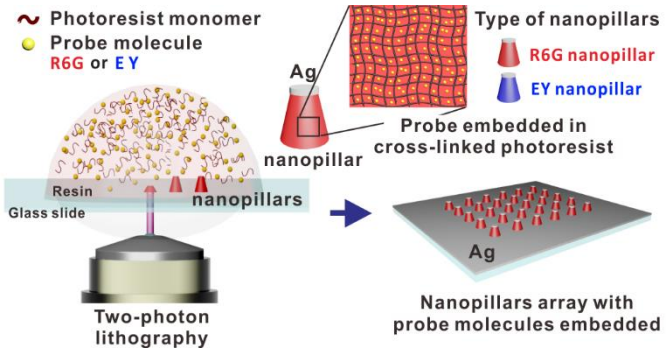

Scheme 1. Fabrication of Ag nanopillars using two-photon photolithography. Left, resin comprising the photoresist and probe molecules (rhodamine 6G, R6G; eosin Y, EY) is drop-cast on a glass slide. The resin is polymerized into pre-defined nanopillar morphology via direct laser writing. Right, Ag nanopillars are fabricated via thermal evaporation. Probe molecules are incorporated into the nanopillars during the laser writing process. Two types of Ag nanopillars (R6G- and EY-encapsulated nanopillars) can be fabricated.

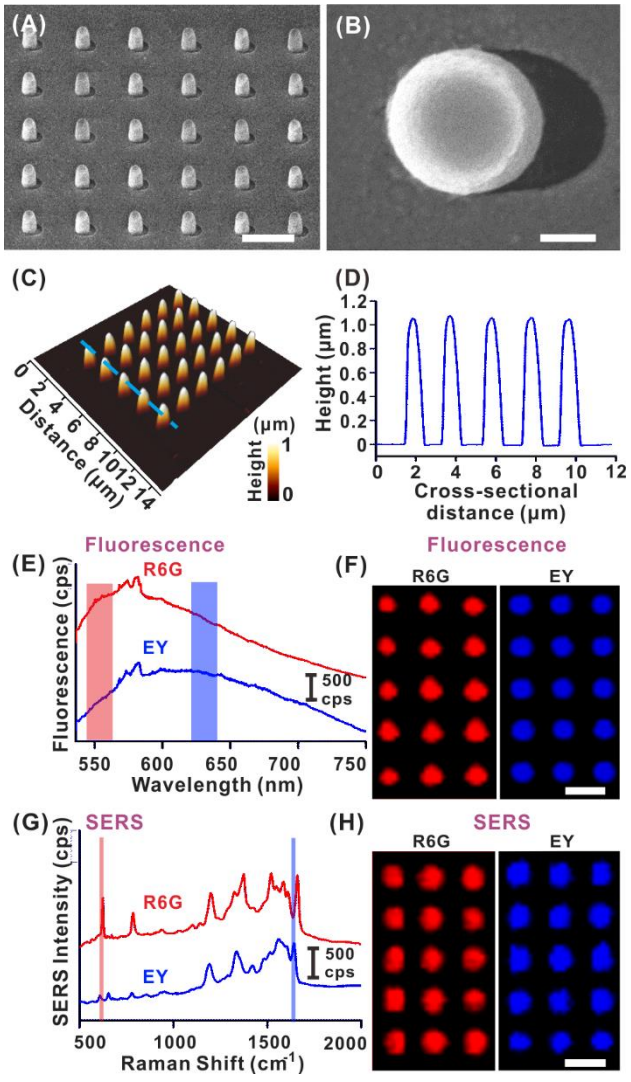

Fig. 1 Dual spectroscopic readout on a single-dye encapsulated nanopillar array. (A, B) SEM and (C, D) AFM images of a 5 × 6 array of nanopillars deposited with Ag film,

respectively. (E) Fluorescence spectra and (F) images taken from R6G- (red) and EY-encapsulated nanopillars (blue), respectively. (G) SERS spectra and (H) images taken from R6G- (red) and EY-encapsulated nanopillars (blue), respectively. Scale bar in (B) represents 200 nm and other scale bars represent 2 µm.

addition to fluorescence read-out, the xy SERS images of R6G-encapsulated nanopillars show the nanopillars exhibiting similar brightness when the characteristic vibrational mode of R6G at 622 cm^{-1} is selected for image generation (Fig. 1G, H, S2Ci, ESI†). Similarly, identical brightness is observed for the EY-encapsulated nanopillars using the 1639 cm^{-1} vibrational fingerprint of EY (Fig. 1G, H, S2Cii, ESI†). A complete vibrational mode assignment of the SERS spectra is given in Tables S1-2.[23-25] The photoresist does not complicate the SERS spectra as compared to commercially available photoresists such as IPL-780 (Fig. S3, ESI†). These observations collectively indicate that our nanopillar platform is capable of using both fluorescence and SERS as read-out techniques for deterring forgery. Notably, this is also the first time in which SERS/fluorescence dual readouts are used for anti-counterfeiting and potentially data storage. Using two spectroscopic readouts in a single anti-counterfeiting platform enhances the complexity of our anti-counterfeiting platform and thus increases the level of security. Compared with the detection-based platforms which can also simultaneously detected SERS and fluorescence, our encoding platform is capable of hiding and locating the dye molecules within the arrays consisting of nanopillars with the same physical features.[26-29] The independency of multiple readouts with physical features enhances the decoding accuracy and increases the security level. Moreover, the encoding strategy is simple and straightforward as compared with the bio-analysis systems.[30-32] Fluorescence and SERS serve as two layers of identification features in our anti-counterfeiting platform and increases the security levels compared with conventional platforms where merely SERS or fluorescence is read out. Furthermore, imaging technique precisely generates unique SERS spectra of molecules encapsulated in each nanopillars, serving as fingerprints of each nanopillars for authentication. Thus, security level can be further enhanced by maximizing the number of nanopillars which can be fully resolved in the hyper-spectral images. This number is defined as information density.

3.2 Information density & grayscale-covert array

An information density of 17,000 pillars per inch can be achieved in a nanopillar array encapsulated with one probe molecule, in which each nanopillar encoded with the molecular information. This information density is determined by the minimum distance between the individual nanopillars which can be fully imaged in the fluorescence/SERS images without significant changes in signal intensities. We determine the information density of our platform by fabricating square arrays of R6G-encapsulated nanopillars with inter-pillar gaps of 3.5, 1.5, 1.0 and 0.5 µm (Fig. 2A-D, S4A-D, ESI†). The corresponding xy SERS/fluorescence images demonstrate that the dye-containing nanopillars need to be spaced at least 1 µm apart from each other (Fig. 2C, S4C, ESI†). Otherwise, at smaller inter-pillar gaps (0.5 µm), the fluorescence/SERS measurements on the array demonstrate un-resolved images and higher signal intensities

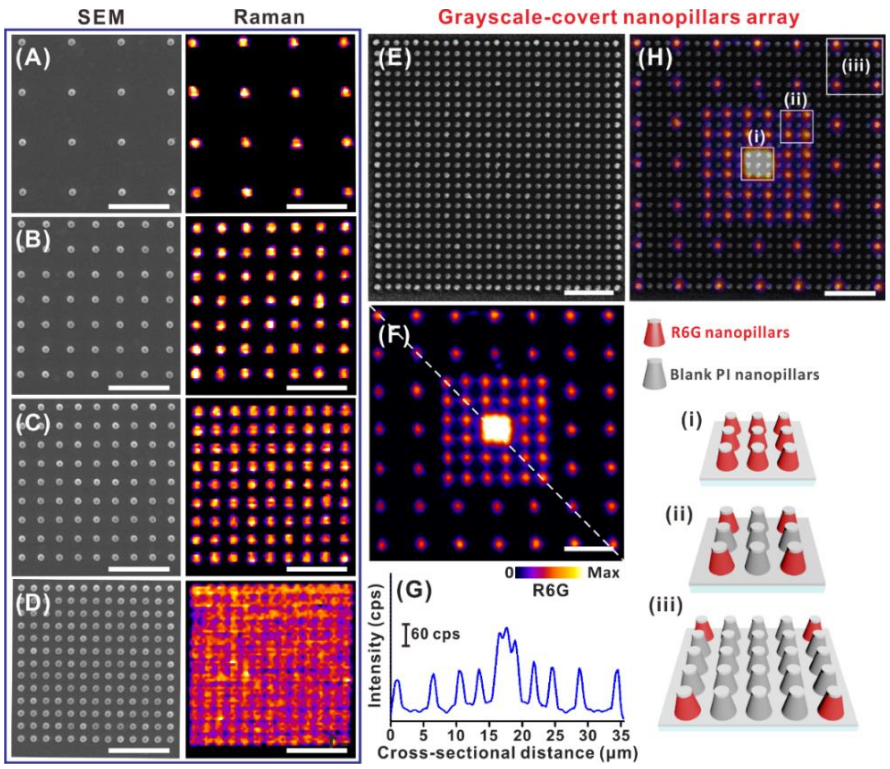

Fig. 2 Information density and intensity grayscales. (A-D) SEM (left) and SERS (right) images of R6G-encapsulated nanopillars with different inter-pillar gaps. The distances between the pillars are (A) 3.5 µm, (B) 1.5 µm, (C) 1 µm and (D) 0.5 µm. An inter-pillar gap of (C) 1 µm is required to fully distinguish the pillar morphology in the SERS images. (D) Un-resolved

SERS images and higher signal intensities are obtained at pillar array with smaller inter-pillar gaps, arising from plasmon coupling and resolution limit of the hyperspectral imaging technique. However, we can make use of this to achieve a three-level signal output to create (E-H) an intensity grayscale. (E) SEM and (F) SERS images of nanopillar array consisting of R6G-encapsulated nanopillars and blank nanopillars. (G) Cross-sectional SERS intensity profiles at diagonal line labeled in (F). (H) Overlaid SERS image and SEM image. The colors in SERS images are assigned by the vibrational signature of R6G at 622 cm-1. All scale bars represent 5 μ m.

compared with other arrays with larger inter-pillar gaps (Fig. 2D, S4D, ESI†). We separately measure the resolution limit of our hyper-spectral imaging technique and the results show two nanopillars should be separated over the length of 0.8-μm in order to be fully resolved in SERS imaging (Fig. S5, ESI†). Below the resolution limit, we observe a signal "spillover" effect that the signals from the side nanopillars are accumulated within the gap region to induce the entire area lighting up as one block (Fig. 2D, S5A and B, ESI†). In all, a density of 17,000 dot per inch is achieved by using our strategy, with each nanopillar representing a dot (Fig. 2C, S4C, ESI †). Our platform outperforms commercial techniques such as inkjet printing, which typically achieves a density of only 1000 – 10000 dot per inch.[33, 34]

Based on the abovementioned inter-pillar-gap dependent outputs, more sophisticated information encoding can be achieved by adding the signal intensities (SERS and fluorescence) as additional information read-out channels in addition to SERS and fluorescence read-outs. To demonstrate this, we fabricate a 25 × 25 array of nanopillars spaced 0.5 μm apart (Fig. 2E). From SEM images, we observe no morphological difference among these nanopillars. In fact, this array consists of R6G-encapsulated nanopillars as the information containing nanopillars and blank nanopillars which act as the 'dummy filler' to shield the positions of real data stored within the nanopillar matrix. The covert information can only be revealed by hyperspectral SERS/fluorescence imaging techniques. The center of this large array is a 3 × 3 array of R6G-encapsulated nanopillars (Fig. 2H-i). This is followed by an 11 × 11 array of R6G-encapsulated and blank nanopillars, where the R6G-encapsulated nanopillars are alternately spaced apart by the blank nanopillars and the separation distance between two R6G-encapsulated nanopillars is 1.5 μm (Fig. 2H-ii). Beyond this, the R6G-encapsulated nanopillars are separated from each other by three blank nanopillars, with a separation distance of 3.5 μm (Fig. 2H-iii).

The corresponding xy SERS image of this array forms a layered concentric square when the 622 cm^{-1} vibrational fingerprint of R6G is selected, showing three levels of intensity output (Fig. 2F). The strongest signals are observed in the center 3 × 3 array of R6G-encapsulated nanopillars at ~ 453 counts per second (cps). The next strongest signal is recorded from the regularly spaced R6G-encapsulated nanopillars in the outer layers at ~ 237 cps (Fig. 2G). Compared with outer-layer arrays (Fig. 2H-ii and -iii), the stronger SERS intensity detected from the center 3 × 3 array (Fig. 2H-i) results from SERS enhancement of double amount of R6G loaded in this array and the "spillover" effect of resolution limit. No R6G signal is observed from the blank nanopillars (Fig. S6, ESI †). By normalizing the SERS intensities from the maximum, a gradient of SERS values at 1, 0.5 and 0 are obtained. A similar signal intensity-based grayscale image (1, 0.5, and 0 intensities) can also be observed in the fluorescence image by selecting the emission peak of R6G at 560 nm (Fig. S4E, ESI†). Thus, we are able to arbitrarily locate these grayscales with three read-outs of information (fluorescence, SERS and signal intensities), by using blank nanopillars which give no R6G signals to control the gaps. Furthermore, these intensity grayscales are covert pieces of information, where normal characterization such as SEM is unable to decode the concentric squares at all (Fig. 2E, F). Consequently, the intensity grayscales as well as their locations serve as additional identification information of complicated security labels to distinguish between authentic and fake products.

3.3 Multiplex array

Next, we develop a multiplex encoding strategy to further enhance the complexity of our nanopillar platform. We selectively encapsulate R6G and EY on different areas of the same nanopillar array using a two-step polymerization process (Fig. 3A), starting with the fabrication of R6G-encapsulated nanopillars. To do so, the individual nanopillars are encoded with their own molecular information. A 4-nm layer of alumina is then deposited over the R6G-encapsulated nanopillars using atomic layer deposition to prevent the R6G molecules from leaching out of the nanopillars. EY-encapsulated nanopillars are subsequently fabricated, followed by thermally evaporating 25 nm of Ag to render the entire substrate SERS active (Fig. S7, ESI †).

Covert information of this multiplex platform can only be fully recovered using hyperspectral SERS imaging. The R6G and EY nanopillars appear structurally identical under normal bright-field microscopic characterization (Fig. 3Bi). The nanopillars light up in the corresponding fluorescence characterization (Fig. 3Bii), indicating that fluorescence can serve as the first identification layer. The covert patterns cannot be fully revealed through fluorescence in this system because of the spectral overlap of broad emission peaks of R6G and EY (Fig. S8, ESI†). Nevertheless, the fluorescence image shows that the emission from the center diamond is stronger than the four corners, because the fluorescence quantum yield of R6G is higher than EY. In contrast, when the vibrational fingerprint of R6G is selected at 622 cm^{-1}, a distinct diamond array can be discerned from the R6G-encapsulated nanopillars; whereas the remaining EY-encoded nanopillars remain invisible (Fig. 3Cii). Conversely, four sets of three nanopillars aligned in a right-angle triangular orientation light up when the vibrational fingerprint of EY at 1639 cm^{-1} is separately selected (Fig. 3Ciii).

The entire square array is formed when a common vibrational mode is selected at 1180 cm-1 (Fig. 3Civ). In anti-counterfeiting terms, the individual SERS images of R6G- and EY-encapsulated nanopillars serve as the second and third identification layers of a security label made by using our nanopillar platform, while the combined image serves as the fourth identification layer to authenticate products. Combining with the tunable intensity grayscales, five identification layers can potentially be used to authenticate genuine products.

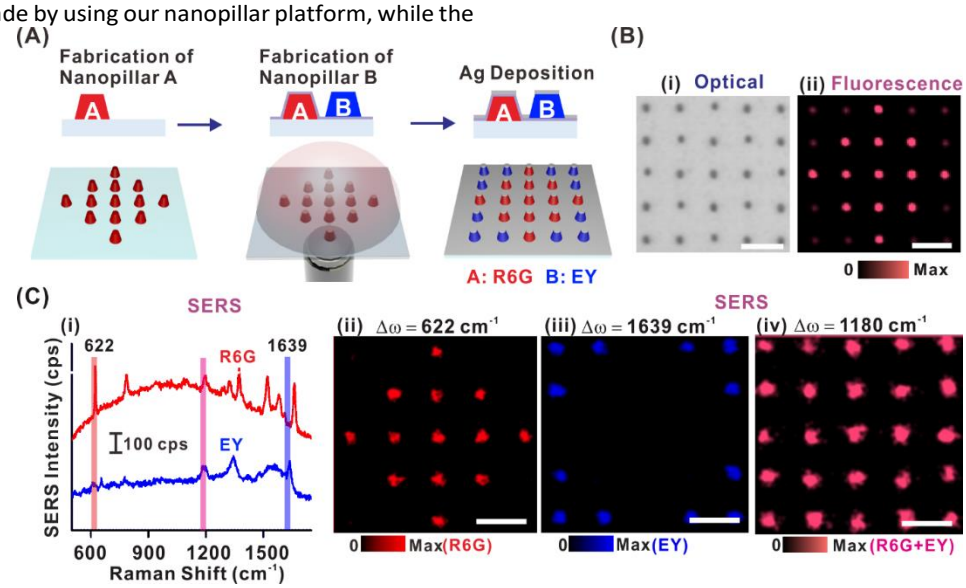

Fig. 3 Multiplex encoding strategy based on spatially selective encapsulation of two dye molecules. (A) Scheme demonstrating the two-step fabrication to selectively encapsulate different probe molecules on the same nanopillar array. (B) (i) bright-field microscopic and (ii) fluorescence images cannot fully reveal the covert structures. (C) (i) SERS spectra and respective SERS images created by selecting at the vibrational bands at (ii) 622 (for R6G), (iii) 1639 (for EY) and (iv) 1180 cm-1, respectively. All scale bars represent 5 µm.

Our multiplex nanopillar platform exhibits a high level of decoding accuracy. The cross-sectional SERS intensity profile at 622 cm^{-1} and 1639 cm^{-1} show uniform signal intensity for both R6G- and EY-encapsulated nanopillars (Fig. S9B, ESI †). Furthermore, we observe no vibrational-mode difference when comparing between the SERS spectra of single dye-encapsulated nanopillars and in the multiplex system (Fig. S10, ESI†). This signal uniformity clearly indicates that the encoded spectral information can be precisely read out without any signal cross-talk in the two-step fabrication process.

3.4 Patterning flexibility

To demonstrate the patterning flexibility of our encoded nanopillars and the high security level of this encoding strategy for potential applications like anti-counterfeiting, we fabricate a “yin-yang” pattern with two symmetric halves comprising R6G- and EY-encapsulated nanopillars. Bright-field microscopic characterization reveals only a solid circle consisting of identical nanopillars (Fig. 4A). Fluorescence image shows the illumination of the whole pattern in which the R6G half is brighter than the EY half, arising from the higher fluorescence quantum yield of R6G. However, SERS image generated using the 622 cm^{-1} peak for R6G can selectively exhibit the left half of ‘yin-yang” (Fig. 4C), whereas selecting at 1639 cm^{-1} for EY exclusively gives rise to the right half of the ‘yin-yang’ (Fig. 4D). It is note-worthy to highlight that the peak difference between 1639 cm^{-1} for EY and 1660 cm^{-1} for R6G is only 21 cm^{-1}, corresponding to ~1 nm spectral gap in the wavelength scale (Fig. S11, ESI†). Thus, the narrow bandwidth of the SERS bands gives rise to a sensitive and accurate anti-counterfeiting platform. The two-layer optical information encoded in this pattern is more complex than security labels revealed by either SERS or fluorescence alone. Furthermore, the hyperspectral imaging technique generates unique SERS fingerprints for every individual R6G- and EY-encapsulated R6G- and EY-encapsulated nanopillar, and this serves as another layer of encryption further deters forgery.

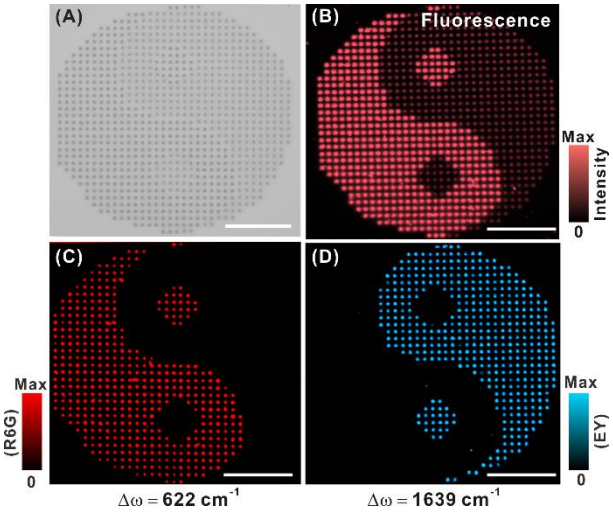

Fig. 4 Multiplex security label consisting of R6G- and EY-encapsulated nanopillars. (A) bright-field microscopic and (B) fluorescence images cannot fully reveal the covert ‘Yin-yang’ symbol. On the other hand, the SERS images created by selecting at (C) 622 cm^{-1} and (D) 1639 cm^{-1} can fully reveal the respective halves of the ‘Yin-yang’ symbol. All scale bars represent 10 µm.

3.5 Data storage capability

In addition to information security, SERS images of the multiplex array demonstrate that the R6G- and EY-encapsulated nanopillars can be individually read out without signal interferences, validating the data storage capability of our nanopillar platform. In total, three well-defined states can be achieved depending on whether it has R6G, EY or no dye molecules encapsulated in nanopillars. To calculate the possible states in terms of data storage, N well-defined states on a data storage platform generate up to NP combinations with P digits. In our platform, N is 3 and P is the number of nanopillars per inch square. Combined with the 17,000 pillar per inch density, our multiplex nanopillar platform is able to provide the total possible states to be $3^{289,000,000}$ states/in^2. We can simultaneously achieve high storage density and secure data protection on a single platform.

Conclusions

In conclusion, we demonstrate a complicated and high-density anti-counterfeiting platform with multiple identification layers which is capable of enhancing information security and deterring product forgery. Molecular Information is hidden behind the same physical features and read out in the form of SERS, fluorescence, and their corresponding signal intensities by using hyperspectral imaging technique. We highlight a spatially selective encapsulation strategy to design various unique and covert patterns within a single array of nanopillars. Full decoding of these patterns require the use of fluorescence and SERS images, and the ability to spectrally resolve 1 nm between extremely closely-spaced vibrational signatures is superior to most conventional optical encryption platforms. Moreover, the use of hyperspectral imaging technology enables retrieving unique SERS spectra from each nanopillars and thus further enhances the security of our platform. Our multiplex nanopillar array is also a potential data storage platform providing the total possible states to be $3^{289,000,000}$ states/in^2. In all, we have shown a progressively complex information encoding platform with large information density, low-error decoding, high flexibility and security. The security level and data storage density can both be enhanced through the use of even more probe molecules or the fabrication of more complex structures.

Acknowledgements

We gratefully thank Prof. Holger Schönherr, Mr. Marc Steuber, and Dr. Ping Li (Universität Siegen) for the fruitful discussion on the synthesis of methyl 2-(methyl(phenyl)amino)acetate. X.Y.L. and Y.H.L. thank the support from National Research Foundation, Singapore (NRF-NRFF2012-04), Nanyang Technological University's start-up grant (M4080758).

References

1 S. Sagiroglu and D. Sinanc, presented in part at 2013 International Conference on Collaboration Technologies and Systems, San Diego, May, 2013.
2 K. Kumar, H. Duan, R. S. Hegde, S. C. Koh, J. N. Wei and J. K. Yang, *Nat. Nanotechnol.*, 2012, **7**, 557-561.
3 X. M. Goh, Y. Zheng, S. J. Tan, L. Zhang, K. Kumar, C.-W. Qiu and J. K. Yang, *Nat. Commun.*, 2014, **5**.
4 S. J. Tan, L. Zhang, D. Zhu, X. M. Goh, Y. M. Wang, K. Kumar, C.-W. Qiu and J. K. Yang, *Nano Lett.*, 2014, **14**, 4023-4029.
5 K. G. Lee, B. G. Choi, B. I. Kim, T. Shyu, M. S. Oh, S. G. Im, S. J. Chang, T. J. Lee, N. A. Kotov and S. J. Lee, *Adv. Mater.*, 2014, **26**, 6119-6124.
6 H. S. Lee, T. S. Shim, H. Hwang, S.-M. Yang and S.-H. Kim, *Chem. Mater.*, 2013, **25**, 2684-2690.
7 L. He, M. Wang, J. Ge and Y. Yin, *Acc. Chem. Res.*, 2012, **45**, 1431-1440.
8 P. Lovera, D. Jones, B. Corbett and A. O'Riordan, *Opt. Express*, 2012, **20**, 25325-25332.
9 H. Ditlbacher, B. Lamprecht, A. Leitner and F. Aussenegg, *Opt. Lett.*, 2000, **25**, 563-565.
10 M. You, J. Zhong, Y. Hong, Z. Duan, M. Lin and F. Xu, *Nanoscale*, 2015, **7**, 4423-4431.
11 Y. Cui, R. S. Hegde, I. Y. Phang, H. K. Lee and X. Y. Ling, *Nanoscale*, 2014, **6**, 282-288.
12 Y. Cui, I. Y. Phang, R. S. Hegde, Y. H. Lee and X. Y. Ling, *ACS Photonics*, 2014, **1**, 631-637.
13 K. J. Si, D. Sikdar, L. W. Yap, J. K. K. Foo, P. Guo, Q. Shi, M. Premaratne and W. Cheng, *Adv. Opt. Mater.*, 2015, **3**, 1710-1717.
14 Y. Lu, J. Zhao, R. Zhang, Y. Liu, D. Liu, E. M. Goldys, X. Yang, P. Xi, A. Sunna and J. Lu, *Nat. Photonics*, 2014, **8**, 32-36.
15 J. Lee, P. W. Bisso, R. L. Srinivas, J. J. Kim, A. J. Swiston and P. S. Doyle, *Nat. Mater.*, 2014, **13**, 524-529.
16 P. Zijlstra, J. W. Chon and M. Gu, *Nature*, 2009, **459**, 410-413.
17 I. Gourevich, H. Pham, J. E. Jonkman and E. Kumacheva, *Chem. Mater.*, 2004, **16**, 1472-1479.
18 L. Bai, Z. Xie, W. Wang, C. Yuan, Y. Zhao, Z. Mu, Q. Zhong and Z. Gu, *ACS nano*, 2014, **8**, 11094-11100.
19 Y. Cui, I. Y. Phang, Y. H. Lee, M. R. Lee, Q. Zhang and X. Y. Ling, *Chem. Commun.*, 2015, **51**, 5363-5366.
20 T. R. Jensen, M. D. Malinsky, C. L. Haynes and R. P. Van Duyne, *J. Phys. Chem. B*, 2000, **104**, 10549-10556.
21 C. Langhammer, B. Kasemo and I. Zorić, *J. Chem. Phys.*, 2007, **126**, 194702.
22 M. Chen and L. Gao, *Inorg. Chem.*, 2006, **45**, 5145-5149.
23 H. Watanabe, N. Hayazawa, Y. Inouye and S. Kawata, *J. Phys. Chem. B*, 2005, **109**, 5012-5020.
24 Y. Q. Wang, S. Ma, Q. Q. Yang and X. J. Li, *Appl. Surf. Sci.*, 2012, **258**, 5881-5885.
25 N. G. Greeneltch, A. S. Davis, N. A. Valley, F. Casadio, G. C. Schatz, R. P. Van Duyne and N. C. Shah, *J. Phys. Chem. A*, 2012, **116**, 11863-11869.
26 L. Rodríguez-Lorenzo, R. A. Alvarez-Puebla, F. J. G. de Abajo and L. M. Liz-Marzán, *J. Phys. Chem. C*, 2009, **114**, 7336-7340.
27 D. Volpati, P. H. Aoki, C. A. Dantas, F. V. Paulovich, M. C. F. de Oliveira, O. N. Oliveira Jr, A. Riul Jr, R. F. Aroca and C. J. Constantino, *Langmuir*, 2011, **28**, 1029-1040.
28 H. Aouani, M. Navarro-Cia, M. Rahmani, T. P. H. Sidiropoulos, M. Hong, R. F. Oulton and S. A. Maier, *Nano Lett.*, 2012, **12**, 4997-5002.
29 G. Lévêque and O. J. F. Martin, *Phys. Rev. Lett.*, 2008, **100**, 117402.
30 S. Lee, H. Chon, S.-Y. Yoon, E. K. Lee, S.-I. Chang, D. W. Lim and J. Choo, *Nanoscale*, 2012, **4**, 124-129.
31 Z. Wang, S. Zong, W. Li, C. Wang, S. Xu, H. Chen and Y. Cui, *J. Am. Chem. Soc.*, 2012, **134**, 2993-3000.
32 S. P. Mulvaney, M. D. Musick, C. D. Keating and M. J. Natan, *Langmuir*, 2003, **19**, 4784-4790.

33 H. Sirringhaus, T. Kawase, R. Friend, T. Shimoda, M. Inbasekaran, W. Wu and E. Woo, *Science*, 2000, **290**, 2123-2126.
34 J.-D. Lee, C.-S. Lee, K.-C. Chun and C.-H. Han, presented in part at Electron Devices Meeting, Washington, DC, December, 1999.

